Geophysical Research Letters

RESEARCH LETTER
10.1029/2018GL077714

Special Section:
Impact of the Sept. 10, 2017, Solar Event on Mars

Responses of the Martian Magnetosphere to an Interplanetary Coronal Mass Ejection: MAVEN Observations and LatHyS Results

N. Romanelli[1], R. Modolo[1], F. Leblanc[2], J.-Y. Chaufray[1], A. Martinez[1], Y. Ma[3], C. O. Lee[4], J. G. Luhmann[4], J. Halekas[5], D. Brain[6], G. DiBraccio[7], J. Espley[7], J. Mcfadden[4], B. Jakosky[6], and M. Holmström[8]

[1]Laboratoire Atmosphères, Milieux et Observations Spatiales, IPSL, CNRS, UVSQ, UPMC, Paris, France, [2]LATMOS/IPSL, UPMC, Université Paris06, Sorbonne Universités, UVSQ, CNRS, Paris, France, [3]Department of Earth, Planetary, and Space Sciences, University of California, Los Angeles, CA, USA, [4]Space Sciences Laboratory, University of California, Berkeley, CA, USA, [5]Department of Physics and Astronomy, University of Iowa, Iowa City, IA, USA, [6]Laboratory for Atmospheric and Space Physics, University of Colorado Boulder, Boulder, CO, USA, [7]NASA Goddard Space Flight Center, Greenbelt, MD, USA, [8]IRF, Kiruna, Sweden

Key Points:
- The interaction between an ICME and Mars is studied by means of MAVEN observations and LatHyS stationary runs
- A characterization of the bow shock compression during this event is performed, based on LatHyS results
- During the analyzed event, simulated H^+ and O^+ planetary loss rates increase by a factor ∼10 and ∼2.4, respectively

Correspondence to:
N. Romanelli,
Norberto.Romanelli@latmos.ipsl.fr

Citation:
Romanelli, N., Modolo, R., Leblanc, F., Chaufray, J.-Y., Martinez, A., Ma, Y., et al. (2018). Responses of the Martian magnetosphere to an interplanetary coronal mass ejection: MAVEN observations and LatHyS results. *Geophysical Research Letters*, *45*. https://doi.org/10.1029/2018GL077714

Received 1 MAR 2018
Accepted 9 MAY 2018
Accepted article online 16 MAY 2018

Abstract The Mars Atmosphere and Volatile EvolutioN (MAVEN) spacecraft observed a strong interplanetary coronal mass ejection (ICME) reaching Mars on 13 September 2017. In this work we analyze the interaction between such an extreme event and the Martian-induced magnetosphere by means of Laboratoire Atmosphères, Milieux et Observations Spatiales Hybrid Simulation (LatHyS) stationary runs and magnetic field and plasma observations obtained by MAVEN in a time interval from ∼ 5 hr before the ICME shock arrival to about 5.5 hr after the impact. Detailed comparisons between simulation results and such MAVEN measurements are performed and show that several stages during this interaction can be described through a combination of steady states. LatHyS results show the simulated bow shock is closer to the planet for higher magnetosonic Mach number and solar wind dynamic pressure conditions, in agreement with previous observational studies. MAVEN observations and LatHyS results also suggest a compression on the flanks of the magnetic pileup boundary. Finally, simulated H^+ and O^+ planetary escape rates increase by a factor ∼10 and ∼2.4, respectively, due to the ICME passage through the Martian magnetosphere.

Plain Language Summary Studies on the responses of Mars to variable external conditions are of great importance, particularly to identify and characterize time-dependent physical processes occurring inside and around its induced planetary magnetosphere. Solar extreme events are expected to play a fundamental role strongly modifying the plasma environment surrounding this atmospheric obstacle, lacking an intrinsic global magnetic field. In this work we analyze the interaction between an interplanetary coronal mass ejection and Mars by means of Mars Atmosphere and Volatile EvolutioN (MAVEN) magnetic field and plasma observations obtained around 13 September 2017. In addition, we study this interacting system by performing three Laboratoire Atmosphères, Milieux et Observations Spatiales Hybrid Simulation stationary runs. Detailed comparisons between simulation results and MAVEN measurements show that several stages during the analyzed time interval can be described through a combination of steady states. In addition, the simulated bow shock is found closer to the planet for higher magnetosonic Mach number and solar wind dynamic pressure conditions. MAVEN observations and Laboratoire Atmosphères, Milieux et Observations Spatiales Hybrid Simulation results also suggest a compression on the flanks of the magnetic pileup boundary. Finally, simulated H+ and O+ planetary escape rates are found to increase by a factor ∼10 and ∼2.4, respectively, due to the interplanetary coronal mass ejection passage through the Martian magnetosphere.

1. Introduction

Interplanetary coronal mass ejections (ICMEs) are large-scale magnetic field and plasma structures with enhanced field magnitude with respect to magnetized background solar wind (SW), and with plasma properties distinct from the SW in which they are embedded (e.g., Gopalswamy, 2006; Jian et al., 2008).

Given their known capability to generate major geomagnetic storms at Earth (e.g., Gosling et al., 1991; Tsurutani & Gonzalez, 1997), and the more direct interaction that takes place between the SW and planets lacking an intrinsic global magnetic field (such as Venus and Mars; Acuña et al., 1998; Russell et al., 1980), ICMEs are expected to play an important role modifying the plasma environment surrounding these atmospheric obstacles.

Studying the Martian response to variable external conditions is of great importance, particularly to identify and characterize time-dependent physical processes occurring inside and around its induced planetary magnetosphere. These studies allow, for instance, to quantify different magnetospheric recovery timescales, to determine related temporal variabilities in each atmospheric escape channel, and to estimate the role that planetary neutral and ion escape to space might have played throughout the history of this planet. However, despite the progress in the understanding of this planetary plasma environment, studies on the responses of the induced magnetosphere of Mars to variability in the external conditions are still required. This is due to the proper limitations of localized spacecraft observations and instrumental design, the computationally expensive time-dependent numerical simulation calculations, and the large amount of nonlinear time-dependent physical processes taking place in such interaction.

The interaction between large ICMEs and the Martian magnetosphere has been studied based on observations provided by Mars Global Surveyor, Mars Express, and Mars Atmosphere and Volatile EvolutioN (MAVEN; Jakosky, Lin, et al., 2015) missions. Results from such investigation can be found in Crider et al. (2005), Curry et al. (2015), Dong et al. (2015), Edberg et al. (2010), Futaana et al. (2008), Jakosky, Grebowsky, et al. (2015), Ma et al. (2017), Morgan et al. (2014), and Sánchez-Cano et al. (2017). Among these studies, Jakosky, Grebowsky, et al. (2015) have shown that ICMEs are capable of increasing the atmospheric planetary escape rate by approximately a factor 10, compared to nominal SW conditions. Consistently with this work, Ma et al. (2017) performed time-dependent magnetohydrodynamic numerical simulations to analyze the rapid changes that took place in the plasma environment around Mars due to these disturbances in the SW and showed that ion escape rates increase by more than one order of magnitude during such event.

In the present work we study the interaction between an ICME that impacted the Martian magnetosphere around 13 September 2017, by means of MAVEN magnetic field and plasma observations. In addition, we also make use of the Laboratoire Atmosphères, Milieux et Observations Spatiales Hybrid Simulation (LatHyS), the Laboratoire de Météorologie Dynamique Global Climate Model (LMD-GCM), and the Exospheric Global Model (EGM) codes to describe the Martian atmosphere, ionosphere, and magnetosphere during this time interval and to study the response of this induced magnetosphere to such extreme event. To do this, we perform three stationary hybrid simulations under estimated external conditions (MAVEN was inside the magnetosphere during this time interval) characterizing different stages of this interacting system. Analysis of Mars Express plasma data during this event is beyond the scope of the present study and will be considered in a future work. After providing a brief description of MAVEN Magnetometer (MAG), Solar Wind Ion Analyzer (SWIA) and Supra-Thermal and Thermal Ion Composition (STATIC) capabilities, and the LatHyS code (section 2), we perform a comparison between MAVEN observations and LatHyS results along the spacecraft trajectory in section 3. We also study the response of the Martian bow shock (BS) and the magnetic pileup boundary (MPB) to the changes in the external conditions due to the passage of the ICME around the induced magnetosphere of Mars. In addition, we estimate the planetary H^+ and O^+ loss rates during this event. In section 4 we provide our conclusions.

2. MAVEN Instruments and LatHyS Code

The MAG instrument provides vector magnetic field measurements with two independent fluxgate magnetometers placed on the end of the solar array panels. They possess a broad range (up to 65,536 nT per axis), a maximum sampling frequency of 32 Hz, and accuracy of ~0.25 nT (Connerney, Espley, DiBraccio, et al., 2015; Connerney, Espley, Lawton, et al., 2015). In this work we have used full time resolution MAG data.

SWIA is an energy and angular ion spectrometer covering an energy range between 25 eV/q and 25 keV/q (with 48 logarithmically spaced energy steps) with a field of view of 360° × 90° (Halekas et al., 2015). In this work we used derived mean plasma density and bulk velocity with 8-s resolution.

Table 1
Solar Wind Properties, IMF, Magnetosonic Mach Number, and SW Dynamic Pressure Considered for Each of Three Simulations During the Corresponding Time Interval

	Simulation 1	Simulation 2	Simulation 3
Time interval	2017-9-12 22:00 UT to 2017-9-13 02:52 UT	2017-9-13 02:52 UT to 2017-9-13 05:10 UT	2017-9-13 05:10 UT to 2017-9-13 08:20 UT
n_{SW} (cm^{-3})	1.9	4	12
$\mathbf{U}_{SW}$ (km/s)	(−426,0,0)	(−824,0,0)	(−824,0,0)
B_{IMF} (nT)	(0,−3,0)	(0,−10,0)	(0,10,5)
M_{MS}	5.15	6.40	8.40
P_{dyn} (nPa)	0.58	4.54	13.61
Bow shock parameters: ε, L (R_M), x_F (R_M)	0.983, 2.195, 0.53	0.915, 1.801, 0.58	0.907, 1.810, 0.55
R^2	0.995	0.998	0.997
Bow shock standoff distance (R_M)	1.64	1.52	1.50
Bow shock terminator distance (R_M)	2.66	2.26	2.24
O^+ escape (10^{24} ions/s)	1.3	1.9	3.1
O^+ escape along the convective electric field (10^{23} ions/s)	1.1	1.9	4.4
H^+ escape (10^{25} ions/s)	2.1	8.2	21.9

Note. Bow shock properties derived from fits to Laboratoire Atmosphères, Milieux et Observations Spatiales Hybrid Simulation results and estimated planetary O^+ and H^+ escape rates are also presented. IMF = interplanetary magnetic field; SW = solar wind.

STATIC is an energy, mass, and angular ion spectrometer, covering an energy range between 0.1 eV/q and 30 keV/q with a field of view of 360° × 90° and a mass range from 1 to 70 amu (McFadden et al., 2015). In this study we have used derived densities for H^+, O^+, O_2^+, and CO_2^+ (from the c6 data product) with 4-s resolution.

LatHyS is a global three-dimensional multispecies parallelized hybrid model that allows to describe plasma processes taking place in several space plasma environments (Leclercq et al., 2016; Modolo et al., 2005, 2012, 2016; Richer et al., 2012). Applied to the Martian environment, it treats six ion species kinetically: SW H_{sw}^+ and He_{sw}^{++}, and planetary H^+, O^+, O_2^+, and CO_2^+. The electrons are described by means of two massless fluids with different temperatures (SW and ionospheric) that ensure the quasi-neutrality condition. The planetary ions are the result of three ionization processes acting on the Martian atmosphere/exosphere (photoionization, charge exchange, and electron impact), several chemical reactions taking place at low altitudes and the self-consistent dynamics (of the ions) by considering model cross sections and ionization frequencies. The description of the crustal magnetic fields at Mars (Acuña et al., 1999) is based on the model derived in Cain et al. (2003). A detailed description of the LatHyS model can be found in Modolo et al. (2016, and references therein). The description of the neutral and ionospheric Martian environment that affect, among other things, the mass-loading conditions of the SW is derived making use of the 3-D LMD-GCM (Chaufray et al., 2014, 2015; González-Galindo et al., 2009) and the 3-D EGM (Leblanc, Chaufray, et al., 2017; Leblanc, Leclercq, et al., 2017).

In this work we perform three stationary numerical simulation runs with 80-km spatial resolution and a time step equal to 0.0333 Ω_{ci}^{-1} where Ω_{ci} is the proton gyrofrequency of the undisturbed SW. The simulation domain extends from −2.4 to 2.4 R_M in X_{MSO} axis and from −4.5 to 4.5 R_M in Y_{MSO} and Z_{MSO} axes (R_M stands for Martian radii, 1 R_M = 3,393 km). The Mars Solar Orbital (MSO) coordinate system is centered at Mars and is defined as follows: the X axis points toward the Sun, the Z axis is perpendicular to Mars's orbital plane and is positive toward the ecliptic north. The Y axis completes the right-handed system. Given that MAVEN is inside the Martian BS during the analyzed time interval, external conditions for the simulation runs are estimated based on MAVEN magnetosheath (MSH) measurements. Considered values for SW density (n_{SW}), mean velocity ($\mathbf{U}_{SW}$), the interplanetary magnetic field (IMF), and the magnetosonic Mach number for each simulation are shown in Table 1. These values, also considered for the three steady state cases analyzed by Ma et al. (2018), are estimated mainly based on penetrating proton measurements (Halekas et al., 2015, 2017). For a more detailed description on this aspect, the reader is referred to sections 3 and 4 of Ma et al. (2018). When it comes to the crustal magnetic fields, it is also worth pointing out that, for each of the three stationary simulations, we have fixed the subsolar geographic (GEO) latitude and longitude at the values taken at

MAVEN's closest approach (CA) during the corresponding time interval. The time interval described by each of these simulations is also reported in this table. The 3-D description of the density, velocity, and temperature of the main neutral and ion species in Mars' thermosphere/ionosphere is determined for solar longitude $Ls = 90°$ and mean solar activity, using the LMD-GCM. Moreover, these outputs are also used to define the background atmosphere and ionosphere of the EGM, and to define Mars' atmosphere in LatHyS model. The reconstructed exospheric composition and density by EGM is used to describe Mars' exosphere in LatHyS model. Although a peak in the Lymann-alpha and in the 0- to 7-nm MAVEN extreme ultraviolet channels are detected on 10 September 2017 between 16:02 and 16:12:45 UT (Thiemann et al., 2018), previous works making use of the LMD-GCM code (Chaufray et al., 2014, 2015) suggest that effects associated with such local maximums do not significantly affect the outcome of LatHyS simulations for the time interval of the present study.

3. MAVEN Observations and LatHyS Results

3.1. Comparison Along MAVEN's Trajectory

Figure 1 displays magnetic field and plasma data obtained by MAVEN MAG, SWIA, and STATIC instruments as a function of time, between 12 September 2017 22:00 UT and 13 September 2017 08:20 UT. From top to bottom, this figure displays the magnetic field vectors in MSO coordinates, total field magnitude, mean plasma velocity components (from SWIA) in MSO coordinates, total plasma velocity, and ion densities derived from STATIC and SWIA. Each panel also shows the corresponding LatHyS results (from the three stationary simulations) along MAVEN's trajectory. As shown in Table 1, the mean IMF considered for the time interval associated with Simulation 1 is $\mathbf{B} = [0, -3, 0]$ nT, that is, a background magnetic field with nominal magnitude upstream from Mars. Moreover, the SW bulk velocity and density corresponding to this time interval are assumed to be $\mathbf{U}_{SW} = [-426, 0, 0]$ km/s and $n_{SW} = 1.9$ cm^{-3}, respectively. Initially, MAVEN is located close to the terminator plane and inside the Martian MSH. It measures strong wave activity, relatively high magnetic field magnitude ($\sim$ 6 nT) and plasma density ($n \sim 4$ cm^{-3}) and smaller plasma bulk velocity ($\sim$240 km/s). As MAVEN moves toward CA at around 12 September 22:54:29 UT, it measures an increase in the magnetic field intensity due to the IMF pileup and the presence of crustal magnetic fields. In addition, a strong decrease in the local plasma velocity and an increase in the total ion density with the major contributions coming from O_2^+ and CO_2^+ are observed. After reaching CA (altitude $\sim$150 km), MAVEN is located downstream and crosses the MPB at the dawn flank at around 23:27 UT, time after which large fluctuations in both magnetic field and mean plasma velocity and density are, once again, detected. Consistent with this transition, STATIC mass spectrogram shows the presence of heavy ions approximately up to this time (not shown in this paper). Even though LatHyS does not capture the fluctuations in **B**, **U**, and n observed in the Martian MSH, the predicted profiles along the spacecraft trajectory are in good agreement with the observed mean values of each of them. Moreover, the IMF draping and pileup, the crustal magnetic fields and correlated changes in the mean plasma velocity field and total plasma density are also well reproduced by LatHyS. These results therefore suggest that MAVEN observations between 12 September 22:00 UT and 13 September 02:52 UT can be understood in terms of nominal draping of magnetic field lines (see, e.g., Chacko & Hassam, 1997; Ma et al., 2004; Modolo et al., 2012; Naor & Keshet, 2015; Romanelli et al., 2014, 2015) and acceleration plasma processes (see, e.g., Dubinin et al., 2011; Halekas et al., 2017), assuming the external conditions reported in Table 1 (Simulation 1).

As can be seen in MAVEN Solar Energetic Particle data, the ICME shock reached the Martian environment at 13 Sept 02:52 UT (Lee et al., 2018). As a result of subsequent changes in the external conditions associated with such extreme event (e.g., increase in the SW dynamic pressure and IMF magnitude), MAVEN observed magnetic field magnitudes significantly larger (maximum being 112.8 nT) around CA (at 13 September 03:20:36 UT), compared with the previous orbit. This increment is not associated with crustal magnetic fields (according to Cain's model (Cain et al., 2003), they are not expected to exceed 15-nT magnitude in this case), but rather associated with a more intense magnetic pileup and draping. As shown in Table 1, we model the 13 September 02:52–05:10 UT time interval by means of a stationary LatHyS run with $\mathbf{B} = [0, -10, 0]$ nT, $\mathbf{U}_{SW} = [-824, 0, 0]$ km/s, and $n_{SW} = 4$ cm^{-3}. Under these external conditions, LatHyS reproduces very well these signatures as well as the deceleration of the plasma and the increase in the total plasma density when MAVEN approaches the ionosphere. After CA, MAVEN observations suggest the spacecraft is inside the MPB until $\sim$03:36 UT. Indeed, although fluctuations in the magnetic field are important even close to CA, heavy ions are not detected after this time (STATIC mass spectrogram). The observed values of the magnetic field components inside the MPB and the MSH (up to 05:10 UT) are well described under a nominal and stationary IMF

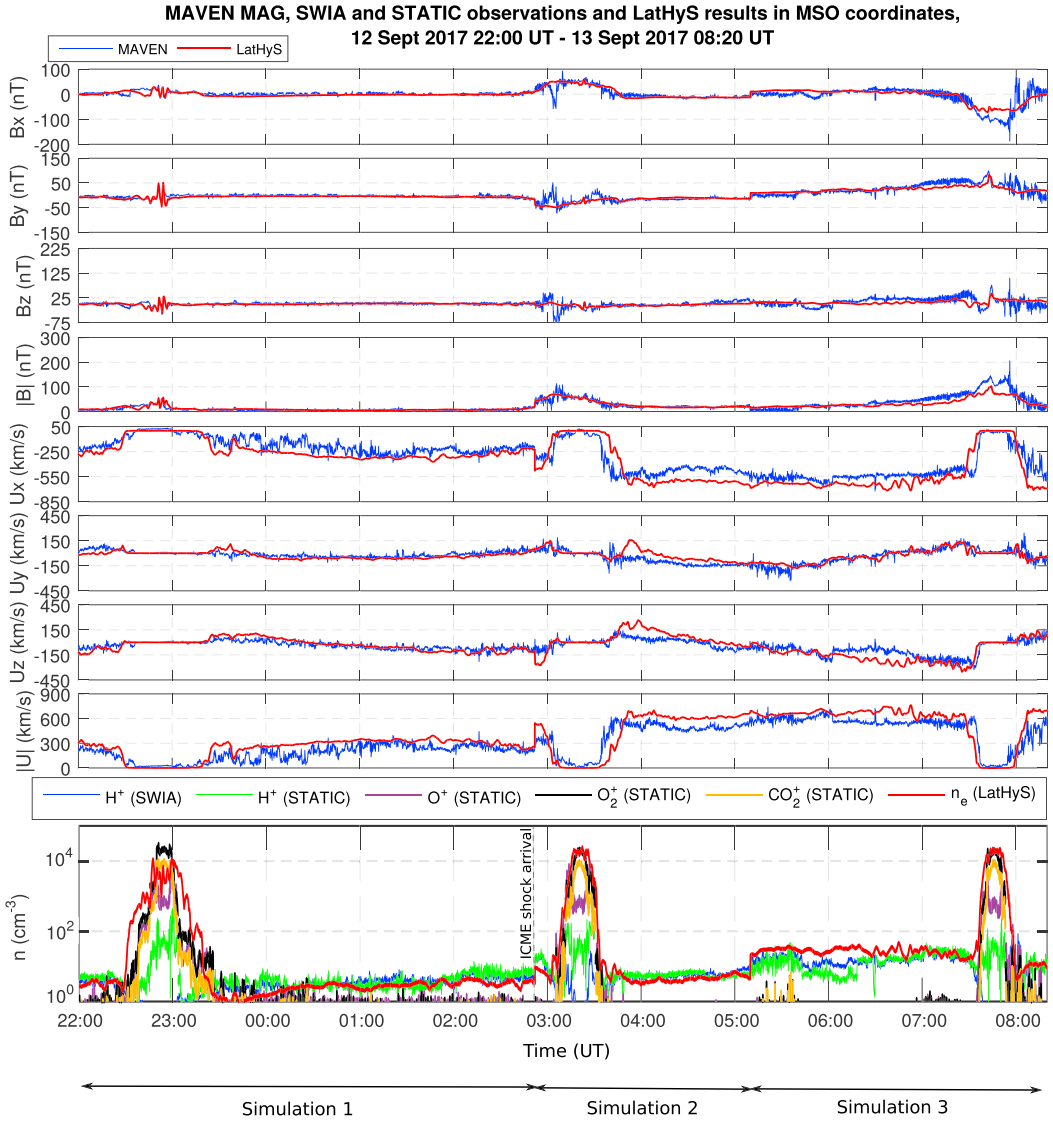

Figure 1. LatHyS results and MAVEN MAG, SWIA, and STATIC observations between 12 September 2017, 22:00 UT, and 13 September 2017, 08:20 UT. From top to bottom: the magnetic field MSO components and magnitude, the SWIA MSO bulk plasma velocity components and magnitude, and the SWIA and STATIC ion densities. LatHyS = Laboratoire Atmosphères, Milieux et Observations Spatiales Hybrid Simulation; MAVEN = Mars Atmosphere and Volatile EvolutioN; MAG = Magnetometer; SWIA = Sola Wind Ion Analyzer; STATIC = Supra-Thermal and Thermal Ion Composition; MSO = Mars Solar Orbital.

draping picture (with the major component along the $-\mathbf{Y}_{MSO}$ axis). Moreover, predicted mean plasma velocities and total densities are also in good agreement with MAVEN SWIA and STATIC measurements during the time interval related to Simulation 2 (see Table 1). However, it is important to notice that physical processes taking place on different timescales are likely present and modify the Martian magnetosphere response to the ICME, when compared to that of under steady state conditions. In particular, the main differences between observations and simulations (between 02:57–03:08 and 03:35–04:00 UT) are examples of such modifications, likely associated with a transient state of the plasma that can only be properly reproduced through time-dependent numerical simulations. In agreement with this idea, simulation results by Ma et al. (2018) suggest MAVEN plasma field velocity during such time intervals can be related to variability in the SW velocity.

At September 13 05:10 UT a sharp change in the local magnetic field By polarity and an increase in the H^+ density are measured by MAVEN. Consistent with these observations, we perform a third stationary numerical simulation with the external conditions presented in Table 1 ($\mathbf{B} = [0, 10, 5]$ nT, $\mathbf{U}_{SW} = [-824, 0, 0]$ km/s,

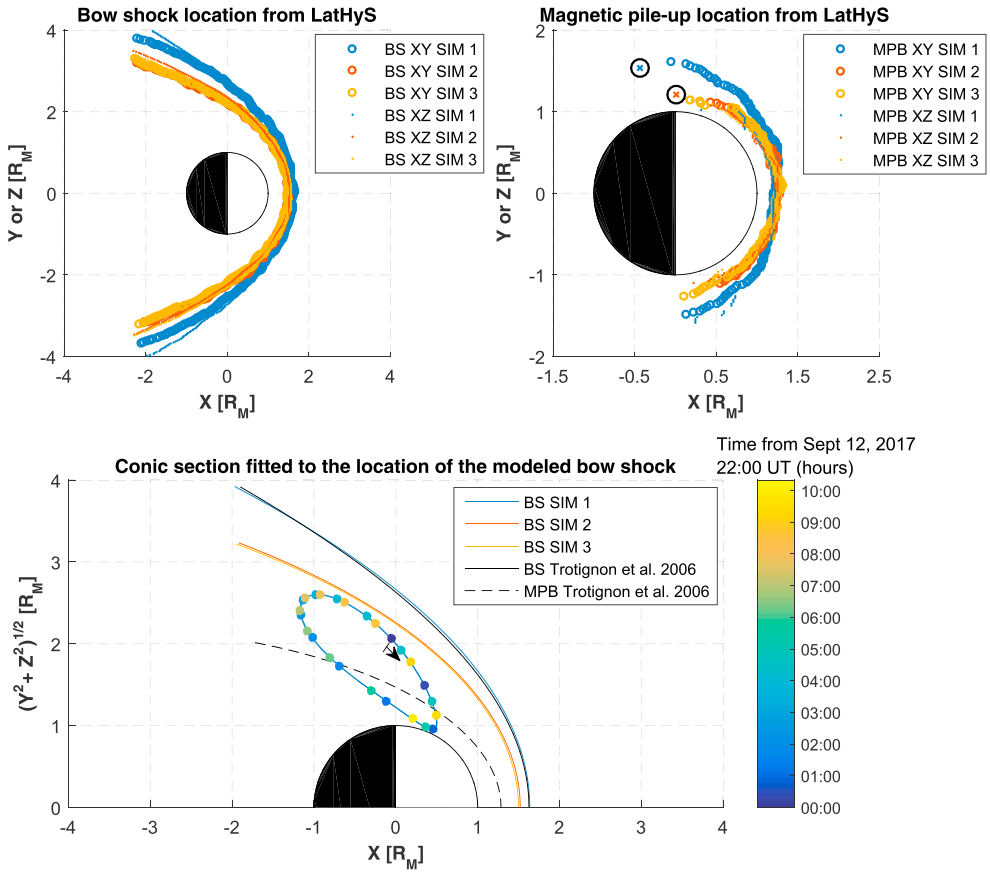

Figure 2. Bow shock (BS) and magnetic pileup location from Laboratoire Atmosphères, Milieux et Observations Spatiales Hybrid Simulation (LatHyS). Upper left (right) panel: bow shock (magnetic pileup boundary, MPB) location in the *X-Y* and *X-Z* Mars Solar Orbital planes for the three stationary simulations. The upper right panel also shows two MPB flank crossings from Mars Atmosphere and Volatile EvolutioN (MAVEN) observations (encircled crosses); see text. Lower panel: Conic section fitted to the location of the modeled bow shock in each of the three simulations, in cylindrical Mars Solar Orbital coordinates. Bow shock and magnetic pileup boundary derived in Trotignon et al. (2006) are also shown, for easy comparison. MAVEN trajectory between 12 September 2017, 22:00 UT, and 13 September 2017, 08:20 UT, is also shown in light blue. The color-coded points display the position of MAVEN at a particular time, every 25 min approximately.

and $n_{SW} = 12$ cm^{-3}). MAVEN observes again a magnetic field configuration consistent with magnetic field draping and pileup under the latter considered IMF orientation and increased SW density. For instance, it is worth noticing the opposite polarity of the Bx and By magnetic field components surrounding the Martian ionosphere, compared to that observed during the previous orbit. This is clearly consistent with the considered change in the IMF direction. Also, the higher magnetic pileup (compared with the previous orbit) can be related to the expected increase in n_{SW}. As in the case of the two previous simulations, the total density predicted by LatHyS along MAVEN's trajectory is very close to that of the dominant species at different times. Indeed, total densities predicted by LatHyS in the Martian ionosphere are in very good agreement with the observed heavy ion densities (e.g., for the maximum in the O_2^+ and/or CO_2^+ densities). Analogously, total density values predicted by LatHyS are in good agreement with protons densities measured by MAVEN when outside of the ionosphere. It is also interesting to notice that LatHyS is capable of reproducing very well the observed changes in the Uy and Uz components, resulting from accelerating processes taking place mainly in the flanks of the Martian MSH. In addition, it is worth pointing out that the presence of high energetic particle fluxes during part of the analyzed event generate an appreciable penetrating background in the SWIA data. Such particle population adds a very hot but tenuous component with zero bulk velocity to these observations. Even though this component artificially increases the density and decreases the flow velocity, it is not expected to strongly affect the overall results presented in Figure 1.

The trajectory of MAVEN during the analyzed time interval is displayed (light blue curve) in cylindrical MSO coordinates in Figure 2 (lower panel). Color-coded points display MAVEN's position every 25 min. This panel also shows the average location of the BS (solid black line) and the MPB (dashed black line), based on the fits by Trotignon et al. (2006). The initial position of MAVEN is marked by the blue dot closest to the black arrow.

3.2. Global Properties Derived From LatHyS

3.2.1. Boundaries Geometry and Location: BS and MPB

Several factors influence the state of the Martian magnetosphere. In particular, previous studies have investigated the effects that changes in the external/internal electromagnetic field and plasma properties (e.g., the SW magnetosonic Mach number, the SW dynamic pressure, the IMF cone angle, the crustal magnetic fields, and the extreme ultraviolet flux reaching the Martian atmosphere) have on the location of the Martian BS and the MPB (e.g., Crider et al., 2003; Edberg et al., 2008, 2009, 2010; Hall et al., 2016). The three stationary simulations allow us to characterize effects that the SW magnetosonic Mach number (M_{MS}) and the SW dynamic pressure (P_{dyn}) have on the BS and MPB location, given that these three simulations were performed for the same solar extreme ultra-violet conditions, and with an IMF mainly oriented along the Y_{MSO} axis. To compute the simulated BS position in each simulation and to also compare it with previous observational results (Trotignon et al., 2006), the following automatic detection criterion has been applied. For a given Y_{MSO} value, we search along the X_{MSO} axis the position where the magnitude of the magnetic field normalized by the IMF magnitude exceeds a factor 2. The first value starting from $X_{MSO} = 2.4\ R_M$ toward the planet (that is along the $-X_{MSO}$ direction) is identified as the BS location for such Y_{MSO} coordinate. The same criteria has been used to compute the location of the BS in the $(X\text{-}Z)_{MSO}$ plane, for each given Z_{MSO} value. A pressure balance criterion between SW thermal and dynamic pressures leads to a similar result in the subsolar region. It fails on the flanks, however, because the MSH plasma is accelerated flankward and tailward, and a simple pressure balance condition is often poorly fulfilled in this region. A similar criterion has been used to compute the MPB location. For each given Y_{MSO} or Z_{MSO} value, we search along the X_{MSO} axis the position where the magnitude of the magnetic field normalized by the IMF magnitude exceeds a factor 6 and the magnitude of the mean plasma velocity normalized by that of the pristine SW is reduced by a factor 2. The identified BS and MPB locations in the *XY* and *XZ* MSO planes (for the three simulations) are shown overimposed in the left and right upper panels in Figure 2, respectively. The simulated MPB profile cannot be completely recovered because the used criteria is not fulfilled everywhere in the simulation box. However, the derived MPB location is extended enough to compare it with previous results. According to Edberg et al. (2008) and Trotignon et al. (2006), the average MPB standoff distance varies between 1.25 ± 0.03 and $1.33 \pm 0.15\ R_M$. As shown in the Figure 2 (upper right panel), all simulated MPB positions have associated standoff distances within such distance range. It is also worth noticing that the computed MPB section close to the terminator plane is significantly closer to the planet when comparing Simulations 2 and 3 with Simulation 1 (close to nominal conditions). This suggests a compression on the MPB flanks, as a result of the SW dynamic pressure and magnetosonic Mach number increase between these simulations (see corresponding values in Table 1). Interestingly, both MPB flank crossings observed by MAVEN that can be accurately determined during the analyzed time interval support such conclusion. Indeed, the blue and red encircled crosses shown in upper right panel (Figure 2) displayed the cylindrical MSO radial distance and the X_{MSO} coordinate of such MPB crossings that took place during the first and second orbits. It is worth mentioning that three additional dayside MPB crossings took place during the analyzed time interval. However, the relatively large magnetic field fluctuations in the magnetic field data as well as the variable plasma composition along MAVEN's trajectory inside the Martian magnetosphere prevent us from accurately determining the MPB crossing location in these cases.

Given that the determined simulated BS profiles are much more extended, we can compute conic section fits to model the BS location assuming cylindrical symmetry along the X_{MSO} axis and using the same methodology reported in Trotignon et al. (2006). The conic section is defined by

$$r = L - \varepsilon r \cos(\theta) \tag{1}$$

where r and θ are the polar coordinates expressed from the conic focus, such that $x - x_F = r\cos(\theta)$ and ε, x_F, and L are the eccentricity, the focus position along the X axis, and the semi-latus rectum (distance of the shock to the focus in the plane perpendicular to the x axis), respectively. The derived values for each of these parameters and the R^2 value associated with the linear fit (from equation (1)) for each of the three simulations are presented in Table 1. As can be seen in this table, the R^2 values are very close to 1, ensuring the derived conic sections fit very well the computed BS location derived from LatHyS. The corresponding conic sections

are displayed in Figure 2 (lower panel). Based on these fits, we also determined the BS standoff distance and the terminator distance (Table 1). We find the computed terminator distance from each simulation to be consistent with the range of values reported in Edberg et al. (2010). Indeed, a decreasing trend (although with large scatter) of the extrapolated terminator distance with the M_{MS} was observed in that study, for magnetosonic Mach numbers ranging between 6.1 and 10.5. As shown in Edberg et al. (2009), the solar dynamic pressure has also a strong influence on the location of the BS and the MPB. An increase in the dynamic pressure was found to push the BS downward, and the presence of an asymptote for relatively large dynamic pressure values was suggested (Figure 6, panel a, of Edberg et al., 2009). Consistent with these observations, we find that BS fits are very similar (e.g., terminator and standoff distance) when comparing Simulations 2 and 3 with Simulation 1. That is, a much larger variability in the BS location is found when P_{dyn} varies between 0.58 and 4.54 nPa than when it varies between 4.54 and 13.61 nPa. While the BS fit for Simulation 1 is very close to the one reported in Trotignon et al. (2006), the standoff and terminator distances are reduced by ~8% and ~15%, respectively, under the conditions for Simulations 2 and 3.

3.2.2. H^+ and O^+ Loss Rates

We also estimate the variability of the H^+ and O^+ planetary loss rates between the three LatHyS stationary runs. As can be seen in Table 1, the H^+ and O^+ loss rates increase by a factor ~ 10 and ~ 2.4, respectively, as a result of the changes in the external conditions during the passage of the ICME through the Martian environment (Simulation 1 versus Simulation 3). These increments are mainly the consequence of an increase in the charge exchange ionization rate between SW protons and H and O atmospheric neutrals (proportional to $n_{SW}\, U_{SW}$). Indeed, in both cases this ionization rate increases by a factor ~12.2. In the case of O^+ escape rates, a significant contribution to such increase is also associated with the motional electric field that can penetrate to lower altitudes due to the increased SW pressure, accelerating and removing ions from the upper layers of the Martian ionosphere. The three LatHyS simulations also show the presence of the O^+ plume in the positive convective electric field hemisphere, as expected from previous observations (e.g., Dong et al., 2015). We find that the ratio between the O^+ escape rate along the convective electric field direction and the total O^+ escape rate increases from Simulation 1 to Simulation 3. Indeed, as shown in Table 1, this O^+ escape channel constitutes ~8.5% and ~14.2% of the total O^+ loss rate for Simulation 1 and Simulation 3, respectively. O_2^+ and CO_2^+ escape rates are not presented in this paper, since the considered spatial resolution might affect the description of physical processes occurring in the ionosphere. Differences in O^+ computed escape rates between LatHyS and magnetohydrodynamic models describing the interaction between ICME events and Mars (e.g., Jakosky, Grebowsky et al., 2015; Ma et al., 2017) might be associated with the considered atmospheric and ionospheric profiles. As mentioned in a previous section, the three LatHyS stationary simulations have used outputs from the LMD-GCM and the EGM codes under mean solar activity conditions and $Ls = 90°$. Such differences can also be partly due to the spatial resolution employed to describe the O^+ ionosphere in LatHyS. Previous estimations of planetary ion escape vary significantly due to different factors: the external conditions, instrumental design, considered hypothesis, and/or employed numerical simulation codes, etc., as can be clearly seen for the case of O^+, in the review by Dubinin et al. (2011). However, it is worth pointing out that the computed total H+ ion loss rate for Simulation 1 is approximately twice the one reported in Modolo et al. (2005), under nominal SW and solar maximum conditions. The derived total O ion loss rate is close to the one reported in Dong et al. (2015) although, in that work based on MAVEN data, the authors focused only on ions with energies higher than 25 eV. Heavy ion escape rate in the same energy range was analyzed in Brain et al. (2015) and was found to exceed 2×10^{24} ions/s. Comparison of these results with ion escape rates associated with Simulations 2 and 3 support the idea that space weather phenomena are capable of having significant effects on the Martian atmospheric escape. Complementary studies on the interaction between Mars and other extreme events can better establish the integrated effect of such impacts over the Martian history.

4. Conclusions

In this work we have analyzed the interaction between an ICME and Mars by means of LatHyS stationary runs and MAVEN measurements obtained during mid-September 2017. Despite that some observations are indicative of the presence of time-dependent processes taking place during the analyzed time interval, comparisons between simulated profiles along the spacecraft trajectory and MAVEN MAG, SWIA, and STATIC observations show a good agreement. This suggests that several stages during this interaction can be partly described through a combination of steady states. We also find that the simulated BS is closer to the planet for higher SW dynamic pressure and magnetosonic Mach number conditions, in agreement with previous

observational studies. The dayside MPB shows much less variability than the BS, although we observe (through MAVEN and LatHyS) a compression on the flanks when the SW dynamic pressure and magnetosonic Mach number increase. Finally, we find that the simulated H^+ and O^+ loss rates increase by a factor ∼10 and ∼2.4, respectively, as a result of the ICME passage through the Martian plasma environment.

Acknowledgments
N. R. is supported by a CDD contract from Laboratoires d'excellence Exploration Spatiale des Environnements Planétaires (LABEX-ESEP ANR 2011-LABX-030). N. R. is also indebted to the French Space Agency CNES for its support. N. R. would like to thank J. Connerney for useful comments and suggestions. N. R., R. M., F. L., and J-Y. C. are indebted to CNRS for its support on the LIA MAGNETO and to ANR for the project TEMPETE (ANR-17-CE31-0016). This work is also part of HELIOSARES Project (ANR-09-BLAN-0223) and ANR MARMITE-CNRS (ANR-13-BS05-0012-02). Authors also acknowledge the support of the IPSL data center CICLAD for providing us access to their computing resources. MAVEN data are publicly available through the Planetary Data System (https://pds-ppi.igpp.ucla.edu/). Numerical simulations outputs used in this article can be found in http://impex.latmos.ipsl.fr.

References

Acuña, M. H., Connerney, J. E. P., Ness, N. F., Lin, R. P., Mitchell, D., Carlson, C. W., et al. (1999). Global distribution of crustal magnetization discovered by the Mars Global Surveyor MAG/ER Experiment. *Science*, *284*, 790–793. https://doi.org/10.1126/science.284.5415.790

Acuña, M. H., Connerney, J. E. P., Wasilewski, P., Lin, R. P., Anderson, K. A., Carlson, C. W., et al. (1998). Magnetic field and plasma observations at Mars: Initial results of the mars global surveyor mission. *Science*, *279*(5357), 1676–1680.

Brain, D. A., Mcfadden, J. P, Halekas, J. S., Connerney, J. E. P., Bougher, S. W., Curry, S., et al. (2015). The spatial distribution of planetary ion fluxes near Mars observed by MAVEN. *Geophysical Research Letters*, *42*, 9142–9148. https://doi.org/10.1002/2015GL065293

Cain, J. C., Ferguson, B. B., & Mozzoni, D. (2003). An $n = 90$ internal potential function of the Martian crustal magnetic field. *Journal of Geophysical Research*, *108*(E2), 5008. https://doi.org/10.1029/2000JE001487

Chacko, Z., & Hassam, A. B. (1997). Steady-state magnetohydrodynamic plasma flow past conducting sphere. *Physics of Plasmas*, *4*(8), 3031–3039. https://doi.org/10.1063/1.872437

Chaufray, J.-Y., Gonzalez-Galindo, F., Forget, F., Lopez-Valverde, M., Leblanc, F., Modolo, R., et al. (2014). Three-dimensional Martian ionosphere model: II. Effect of transport processes due to pressure gradients. *Journal of Geophysical Research: Planets*, *119*, 1614–1636. https://doi.org/10.1002/2013JE004551

Chaufray, J.-Y., Gonzalez-Galindo, F., Forget, F., Lopez-Valverde, M. A., Leblanc, F., Modolo, R., & Hess, S. (2015). Variability of the hydrogen in the Martian upper atmosphere as simulated by a 3D atmosphere-exosphere coupling. *Icarus*, *245*, 282–294. https://doi.org/10.1016/j.icarus.2014.08.038

Connerney, J. E. P., Espley, J. R., DiBraccio, G. A., Gruesbeck, J. R., Oliversen, R. J., Mitchell, D. L., et al. (2015). First results of the MAVEN magnetic field investigation. *Geophysical Research Letters*, *42*, 8819–8827. https://doi.org/10.1002/2015GL065366

Connerney, J. E. P., Espley, J., Lawton, P., Murphy, S., Odom, J., Oliversen, R., & Sheppard, D. (2015). The MAVEN magnetic field investigation. *Space Science Reviews*, *195*, 257–291. https://doi.org/10.1007/s11214-015-0169-4

Crider, D. H., Espley, J., Brain, D. A., Mitchell, D. L., Connerney, J. E. P., & Acuña, M. H. (2005). Mars Global Surveyor observations of the Halloween 2003 solar superstorm's encounter with Mars. *Journal of Geophysical Research*, *110*, A09S21. https://doi.org/10.1029/2004JA010881

Crider, D. H., Vignes, D., Krymskii, A. M., Breus, T. K., Ness, N. F., Mitchell, D. L., et al. (2003). A proxy for determining solar wind dynamic pressure at Mars using Mars Global Surveyor data. *Journal of Geophysical Research*, *108*(A12), 1461. https://doi.org/10.1029/2003JA009875

Curry, S. M., Luhmann, J. G., Ma, Y. J., Dong, C. F., Brain, D., Leblanc, F., et al. (2015). Response of Mars O^+ pickup ions to the 8 March 2015 ICME: Inferences from MAVEN data-based models. *Geophysical Research Letters*, *42*, 9095–9102. https://doi.org/10.1002/2015GL065304

Dong, C., Ma, Y., Bougher, S. W., Toth, G., Nagy, A. F., Halekas, J. S., et al. (2015). Multifluid MHD study of the solar wind interaction with Mars' upper atmosphere during the 2015 March 8th ICME event. *Geophysical Research Letters*, *42*, 9103–9112. https://doi.org/10.1002/2015GL065944

Dubinin, E., Fraenz, M., Fedorov, A., Lundin, R., Edberg, N., Duru, F., & Vaisberg, O. (2011). Ion energization and escape on Mars and Venus. *Space Science Reviews*, *162*, 173–211. https://doi.org/10.1007/s11214-011-9831-7

Edberg, N. J. T., Brain, D. A., Lester, M., Cowley, S. W. H., Modolo, R., Fränz, M., & Barabash, S. (2009). Plasma boundary variability at Mars as observed by Mars Global Surveyor and Mars Express. *Annals of Geophysics*, *27*(9), 3537–3550.

Edberg, N. J. T., Lester, M., Cowley, S. W. H., Brain, D. A., Fränz, M., & Barabash, S. (2010). Magnetosonic Mach number effect of the position of the bow shock at Mars in comparison to Venus. *Journal of Geophysical Research*, *115*, A07203. https://doi.org/10.1029/2009JA014998

Edberg, N. J. T., Lester, M., Cowley, S. W. H., & Eriksson, A. I. (2008). Statistical analysis of the location of the Martian magnetic pileup boundary and bow shock and the influence of crustal magnetic fields. *Journal of Geophysical Research*, *113*, A08206. https://doi.org/10.1029/2008JA013096

Futaana Y., Barabash, S., Yamauchi, M., McKenna-Lawlor, S., Lundin, R., Luhmann, J. G., et al. (2008). Mars Express and Venus Express multi-point observations of geo-effective solar flare events in December 2006. *Planetary and Space Science*, *56*(6), 873–880. https://doi.org/10.1016/j.pss.2007.10.014

González-Galindo, F., Forget, F., López-Valverde, M. A., Angelats i Coll, M., & Millour, E. (2009). A ground-to-exosphere Martian circulation model: 1. Seasonal, diurnal, and solar cycle variation of thermospheric temperatures. *Journal of Geophysical Research*, *114*, E04001. https://doi.org/10.1029/2008JE003246

Gopalswamy, N. (2006). Properties of interplanetary coronal mass ejections. *Space Science Reviews*, *124*, 145–168. https://doi.org/10.1007/s11214-006-9102-1

Gosling, J., McComas, D., Phillips, J., & Bame, S. (1991). Geomagnetic activity associated with Earth passage of interplanetary shock disturbances and coronal mass ejections. *Journal of Geophysical Research*, *96*(A5), 7831–7839. https://doi.org/10.1029/91JA00316

Halekas, J. S., Brain, D. A., Luhmann, J. G., DiBraccio, G. A., Ruhunusiri, S., Harada, Y., & Jakosky, B. M. (2017). Flows, fields, and forces in the Mars-solar wind interaction. *Journal of Geophysical Research: Space Physics*, *122*, 11,320–11,341. https://doi.org/10.1002/2017JA024772

Halekas, J. S., Taylor, E. R., Dalton, G., Johnson, G., Curtis, D. W., McFadden, J. P., et al. (2015). *The solar wind ion analyzer for MAVEN* (Vol. 195, pp. 125–151). https://doi.org/10.1007/s11214-013-0029-z

Hall, B. E. S., Lester, M., Sánchez-Cano, B., Nichols, J. D., Andrews, D. J., Edberg, N. J. T., et al. (2016). Annual variations in the Martian bow shock location as observed by the Mars Express mission. *Journal Geophysical Research: Space Physics*, *121*, 11,474–11,494. https://doi.org/10.1002/2016JA023316

Jakosky, B. M., Grebowsky, J. M., Luhmann, J. G., Connerney, J., Eparvier, F., Ergun, R., et al. (2015). MAVEN observations of the response of Mars to an interplanetary coronal mass ejection. *American Association for the Advancement of Science*, *350*(6261), aad0210-1–aad0210-7. https://doi.org/10.1126/science.aad0210

Jakosky, B. M., Lin, R. P., Grebowsky, J. M., Luhmann, J. G., Mitchell, D. F., Beutelschies, G., et al. (2015). The Mars Atmosphere and Volatile Evolution (MAVEN) mission. *Space Science Reviews*, *195*(1-4), 3–48. https://doi.org/10.1007/s11214-015-0139-x

Jian, L. K., Russell, C. T., Luhmann, J. G., Skoug, R. M., & Steinberg, J. T. (2008). Stream interactions and interplanetary coronal mass ejections at 5.3 AU near the solar ecliptic plane. *Solar Physics*, *250*, 375–402. https://doi.org/10.1007/s11207-008-9204-x

Leblanc, F., Chaufray, J. Y., Modolo, R., Leclercq, L., Curry, S., Luhmann, J., & Jakosky, B. (2017). On the origins of Mars' exospheric nonthermal oxygen component as observed by MAVEN and modeled by HELIOSARES. *Journal of Geophysical Research: Planets*, *122*, 2401–2428. https://doi.org/10.1002/2017JE005336

Leblanc, F., Leclercq, L., Oza, A., Schmidt, C., Modolo, R., Chaufray, J. Y., & Johnson, R. E. (2017). 3D multispecies collisional model of Ganymede's atmosphere. *Icarus*, *293*, 185–198. https://doi.org/10.1016/j.icarus.2017.04.025

Leclercq, L., Modolo, R., Leblanc, F., Hess, S., & Mancini, M. (2016). 3D magnetospheric parallel hybrid multi-grid method applied to planet-plasma interactions. *Journal of Computational Physics*, *309*, 295–313. https://doi.org/10.1016/j.jcp.2016.01.005

Lee, C. O., Jakosky, B. M., Luhmann, J. G., Brain, D. A., Mays, M. L., Hassler, D. M., et al. (2018). Observations and impacts of the 10 September 2017 solar events at Mars: An overview and synthesis of the initial results. *Geophysical Research Letters,* https://doi.org/10.1029/2018GL079162

Ma, Y., Fang, X., Halekas, J. S., Xu, S., Russell, C. T., Luhmann, J. G., et al. (2018). The Impact and Solar Wind Proxy of the 2017 September ICME Event at Mars. *Geophysical Research Letters*, *45*. https://doi.org/10.1029/2018GL077707

Ma, Y., Nagy, A. F., Sokolov, I. V., & Hansen, K. C. (2004). Three-dimensional, multispecies, high spatial resolution MHD studies of the solar wind interaction with Mars. *Journal of Geophysical Research*, *109*, A07211. https://doi.org/10.1029/2003JA010367

Ma, Y. J., Russell, C. T., Fang, X., Dong, Y., Nagy, A. F., Toth, G., et al. (2017). Variations of the Martian plasma environment during the ICME passage on 8 March 2015: A time-dependent MHD study. *Journal of Geophysical Research: Space Physics*, *122*, 1714–1730. https://doi.org/10.1002/2016JA023402

McFadden, J., Kortmann, O., Curtis, D., Dalton, G., Johnson, G., Abiad, R., et al. (2015). MAVEN Suprathermal and thermal Ion Composition (STATIC) instrument. *Space Science Reviews*, *195*, 199–256. https://doi.org/10.1007/s11214-015-0175-6

Modolo, R., Chanteur, G. M., & Dubinin, E. (2012). Dynamic Martian magnetosphere: Transient twist induced by a rotation of the IMF. *Geophysical Research Letters*, *39*, L01106. https://doi.org/10.1029/2011GL049895

Modolo, R., Chanteur, G. M., Dubinin, E., & Matthews, A. P. (2005). Influence of the solar EUV flux on the Martian plasma environment. *Annales de Geophysique*, *23*, 433–444. https://doi.org/10.5194/angeo-23-433-2005

Modolo, R., Hess, S., Mancini, M., Leblanc, F., Chaufray, J.-Y., Brain, D., et al. (2016). Mars-solar wind interaction: LatHyS, an improved parallel 3-D multispecies hybrid model. *Journal of Geophysical Research: Space Physics*, *121*, 6378–6399. https://doi.org/10.1002/2015JA022324

Morgan, D. D., Diéval, C., Gurnett, D. A., Duru, F., Dubinin, E. M., Fränz, M., et al. (2014). Effects of a strong ICME on the Martian ionosphere as detected by Mars Express and Mars Odyssey. *Journal of Geophysical Research: Space Physics*, *119*, 5891–5908. https://doi.org/10.1002/2013JA019522

Naor, Y., & Keshet, U. (2015). Magnetohydrodynamics using path or stream functions. *The Astrophysical Journal*, *810*, 152.

Richer, E., Modolo, R., Chanteur, G. M., Hess, S., & Leblanc, F. (2012). A global hybrid model for Mercury's interaction with the solar wind: Case study of the dipole representation. *Journal of Geophysical Research*, *117*, A10228. https://doi.org/10.1029/2012JA017898

Romanelli, N., Bertucci, C., Gómez, D., & Mazelle, C. (2015). Dependence of the location of the Martian magnetic lobes on the interplanetary magnetic field direction: Observations from Mars Global Surveyor. *Journal of Geophysical Research: Space Physics*, *120*, 7737–7747. https://doi.org/10.1002/2015JA021359

Romanelli, N., Gómez, D., Bertucci, C., & Delva, M. (2014). Steady-state magnetohydrodynamic flow around an unmagnetized conducting sphere. *The Astrophysical Journal*, *789*(1), 1–7.

Russell, C. T., Elphic, R. C., & Slavin, J. A. (1980). Limits on the possible intrinsic magnetic field of Venus. *Journal of Geophysical Research*, *85*, 8319–8332.

Sánchez-Cano, B., Hall, B. E. S., Lester, M., Mays, M. L., Witasse, O., Ambrosi, R., et al. (2017). Mars plasma system response to solar wind disturbances during solar minimum. *Journal of Geophysical Research: Space Physics*, *122*, 6611–6634. https://doi.org/10.1002/2016JA023587

Thiemann, E. M. B., Andersson, L., Lillis, R., Withers, P., Xu, S., Elrod, M., et al. (2018). The Mars Topside Ionosphere Response to the X8.2 Solar Flare of 10 September 2017. *Geophysical Research Letters*, *45*. https://doi.org/10.1029/2018GL077730

Trotignon, J. G., Mazelle, C., Bertucci, C., & Acuña, M. H. (2006). Martian shock and magnetic pile-up boundary positions and shapes determined from the Phobos 2 and Mars Global Surveyor data sets. *Planetary and Space Science*, *54*, 357–369. https://doi.org/10.1016/j.pss.2006.01.003

Tsurutani, B., & Gonzalez, W. (1997). The interplanetary causes of magnetic storms: A review. In B. T. Tsurutani et al. (Eds.), *Magnetic Storms, Geophysical Monograph Series* (Vol. 98, pp. 77–89). Washington, DC: American Geophysical Union.